Condensed Matter Physics.
Dielectrics

Dielectric spectroscopy of a 10% solution of human immunoglobulin G at physiological temperatures. Part 1

Zh. A. Salnikova [✉1], A. P. Smirnov [1], R. A. Castro Arata [1]

[1] Herzen State Pedagogical University of Russia, 48 Moika Emb., Saint Petersburg 191186, Russia

Authors

Zhanna A. Salnikova, ORCID: 0000-0002-8244-7513, e-mail: jannete90@mail.ru

Alexander P. Smirnov, ORCID: 0000-0003-2463-2056, e-mail: Smirnov_Alexander_hspu@mail.ru

Rene Alejandro Castro Arata, ORCID: 0000-0002-1902-5801, e-mail: recastro@mail.ru

Abstract. In this paper, the dielectric and relaxation properties of a 10% water solution of human immunoglobulin are investigated in the frequency range of 0.1 Hz to 15 MHz at temperatures between 35 and 39.7 °C. The frequency dependences of the dielectric loss factor ε'' were obtained, revealing three maxima in the dispersion regions ε'. These maxima were approximated by the Havriliak–Negami equation. For each relaxation process, the parameters α, β, and τ_0 were calculated at different temperatures, and the time distribution functions of the relaxers, G(t), were derived. The paper proposes possible interpretations of the kinetic units responsible for these processes and discusses potential phase transitions within the system.

Keywords: dielectric constant of immunoglobulin G, dielectric losses of IgG, relaxation parameters of IgG, Havriliak–Negami equation, phase transitions, globule–tangle, immunoglobulins

Introduction

In the physics of dielectrics, the method of dielectric spectroscopy is widely used for comprehensive studies of the frequency dependences of the dielectric constant $\varepsilon'(f)$ and the dielectric loss factor $\varepsilon''(f)$. The fundamental principles of this method are well-documented in both domestic and international educational and scientific literature. See, for example (Borisova, Koikov 1979; Gorokhovatskiy et al. 2013; Kremer, Schönhals 2003). This technique has been applied to investigate synthetic polymer dielectrics as well as biological objects (Blythe, Bloor 2005; Sazhin 1986; Annus, Min 2021; Raicu, Feldman 2015). The relaxation parameters of dielectrics are determined from the maxima observed in the frequency dependence of the dielectric loss factor and are typically analyzed using the Havriliak — Negami equation. From this analysis, the relaxation parameters α, β, and τ_0 are obtained at various temperatures, the time distribution functions of the relaxers, $G(\tau)$, are derived, and the activation energy E_a of the dipole polarization process is calculated.

In this work, the object of the study is a 10% aqueous solution of human immunoglobulin G (IgG). The purpose of this study is to investigate the dielectric characteristics and relaxation parameters of the sample across a broad frequency range at physiological temperatures, followed by comprehensive analysis of the obtained results.

Relaxation equations

To analyze the relaxation properties of dielectrics, we employ the concept of complex dielectric constant ε^*, defines as:

$$\varepsilon^*(\omega) = \varepsilon'(\omega) - i\cdot\varepsilon''(\omega), \tag{1}$$

where ω is the cyclic frequency of the applied electric field, $\varepsilon'(\omega)$ denotes the real part (permittivity of the medium) characterizing the medium's ability to shield an external electric field, $\varepsilon''(\omega)$ represents the imaginary part (dielectric loss factor) describing energy absorption and its conversion to thermal energy.

Relaxation phenomena are generally described by the Havriliak–Negami equation (H–N) (Kremer, Schönhals 2003, 62) (we used in the formula $1 - \alpha$, $1 - \beta$):

$$\varepsilon^*(\omega) = \varepsilon_\infty + \frac{\varepsilon_s - \varepsilon_\infty}{(1+(i\omega\tau_0)^{1-\alpha})^{1-\beta}}, \tag{2}$$

where ε_s, ε_∞ are the static and high–frequency dielectric constant $\varepsilon'(\omega)$ (ε_s – at $\omega \to 0$, ε_∞ – at $\omega \to \infty$), τ_0 is the most probable relaxation time of the sample molecules (or their individual kinetic units), α is the width of the relaxation time spectrum, β is the dissymmetry of this spectrum. These parameters vary within the following limits: $0 \le \alpha < 1$, $0 \le \beta < 1$. The greater the value α, the greater the spread of relaxation times of the sample molecules τ relative to τ_0, that is, the wider the relaxation spectrum (therefore, the value $1 - \alpha$ is used in the formula in this work); the greater β, the greater the degree of its dissymmetry (therefore, we use the value $1 - \beta$ in the formula). For such complex systems as aqueous solutions of biopolymers, the α parameter and, especially, the β parameter are significantly higher than for low molecular weight compounds.

When considering the sample molecules as independent dipoles with several discrete orientation states, it is concluded that there are molecules with different relaxation times τ (Fröhlich 1958). The distribution of molecules with different τ relative to τ_0 is described by the function $G(\tau)$ (Kremer, Schönhals 2003, 62):

$$G(\tau) = \frac{\left(\frac{\tau}{\tau_0}\right)^{\beta(1-\alpha)} \sin\left((1-\beta)\theta\right)}{\pi\tau\left[\left(\frac{\tau}{\tau_0}\right)^{2(1-\alpha)} + 2\left(\frac{\tau}{\tau_0}\right)^{(1-\alpha)}\cos(\pi(1-\alpha)) + 1\right]^{\frac{1-\beta}{2}}}, \tag{3}$$

where: $\theta = arctg\left[\dfrac{\sin\left(\pi(1-\alpha)\right)}{\left(\frac{\tau}{\tau_0}\right)^{(1-\alpha)} + \cos(\pi(1-\alpha))}\right]$ and $0 \le \theta \le \pi$.

At $\alpha = 0$ and $\beta = 0$, the H–N equation becomes the Debye equation (Kremer, Schönhals 2003, 62):

$$\varepsilon^*(\omega) = \varepsilon_\infty + \frac{\varepsilon_s - \varepsilon_\infty}{1 + i\omega\tau_0}, \tag{4}$$

In this case, $G(\tau)$ is a delta function $\delta(\tau_0)$, which corresponds to the state when all kinetic units of the sample have the same relaxation time τ_0.

At $\alpha \ne 0$ and $\beta = 0$, the H–N equation becomes the Cole–Cole equation (Kremer, Schönhals 2003, 62):

$$\varepsilon^*(\omega) = \varepsilon_\infty + \frac{\varepsilon_s - \varepsilon_\infty}{1 + (i\omega\tau_0)^{1-\alpha}}, \tag{5}$$

Here $G(\tau)$ is a symmetric function with respect to τ_0.

At $\alpha = 0$ and $\beta \neq 0$, the H–N equation becomes the Davidson–Cole equation (Kremer, Schönhals 2003, 62):

$$\varepsilon^*(\omega) = \varepsilon_\infty + \frac{\varepsilon_s - \varepsilon_\infty}{(1 + i\omega\tau_0)^{1-\beta}}, \tag{6}$$

In this case, $G(\tau)$ is an asymmetric function with respect to τ_0.

The parameters α, β, and τ_0 are the main relaxation parameters of the object of study.

The parameter α characterizes how strongly the relaxation times τ of the kinetic units of a given relaxation process differ in frequency. The more kinetic units with different relaxation times, the greater the α. The parameter β determines the cooperative nature of the reorientation of kinetic units, considered as dipoles that make abrupt turns under the influence of an external field, in which the probability of reorientation of the kinetic unit and the activation energy depend on the orientation of the neighbors. The stronger the dependence on the orientation of the neighbors, the greater the β.

Method for determining relaxation parameters α, β, and τ_0

From equation H–N (2) and considering the aforementioned theoretical framework, we derive the equation for $\varepsilon''(\omega)$ (Salnikova, Kononov 2020):

$$\varepsilon''(\omega) = \frac{(\varepsilon_s - \varepsilon_\infty) \cdot \sin(1-\beta)\varphi}{[1 + 2(\omega\tau_0)^{1-\alpha} \sin\frac{\pi\alpha}{2} + (\omega\tau_0)^{2(1-\alpha)}]^{\frac{1-\beta}{2}}}, \tag{7}$$

where $\varphi = arctg[\dfrac{(\omega\tau_0)^{1-\alpha} \cos\dfrac{\pi\alpha}{2}}{1 + (\omega\tau_0)^{1-\alpha} \sin\dfrac{\pi\alpha}{2}}]$.

Experimentally measured quantities are usually $\varepsilon'(\omega)$ and $\varepsilon''(\omega)$. At the same time, a dispersion is observed on the graph $\varepsilon'(\omega)$, and a maximum in the frequency band of the dispersion $\varepsilon'(\omega)$ is observed on the graph $\varepsilon''(\omega)$. The relaxation parameters α, β, and τ_0 are determined empirically at each temperature, from the principle of the best approximation of the experimental values $\varepsilon''(\omega)$ by the graph $\varepsilon''(\omega)$ according to formula (7). When constructing an approximating curve for the graph $\varepsilon''(\omega)$, the least squares method is used. Having obtained the values α, β and τ_0, the relaxation time distribution function of the molecules of the sample $G(\tau)$ is constructed according to formula (3).

In the presence of several relaxation processes, as well as in the presence of electrical conductivity of the sample, the H–N equation is used in a generalized form:

$$\varepsilon^*(\omega) = -i\left(\frac{\sigma_0}{\varepsilon_0\omega}\right)^s + \sum_{k=1}^{3}\left[\frac{\varepsilon_{sk} - \varepsilon_{\infty k}}{(1 + (i\omega\tau_k)^{1-\alpha_k})^{1-\beta_k}} + \varepsilon_{\infty k}\right] \tag{8}$$

This formula takes into account three relaxation processes, with the first term accounting for electrical conductivity effects. The parameters are the same as in formula (2), σ_0 is the electrical conductivity at the minimum frequency under study, s is the exponent $0 \leq s \leq 1$, ε_0 is the dielectric constant ($\varepsilon_0 = 8.85 \cdot 10^{-12}$ F/m).

Proteins exhibit a broad spectrum of motional modes across multiple structural scales — including quaternary, tertiary, secondary, and primary structure rearrangements — each characterized by distinct activation barriers and characteristic timescales. Motional modes with comparable relaxation times may be collectively described as a single relaxation process (Gotlib et al. 1986, 156), though this aggregation typically results in a markedly asymmetric relaxation time distribution function $G(\tau)$ (Gotlib et al. 1986, 159). This behavior manifests experimentally as a broad and asymmetric relaxation spectrum on the graph $\varepsilon''(f)$.

Experiment

Samples

The experimental samples consisted of human normal immunoglobulin produced by NPO Microgen JSC (Moscow, Russia), obtained through standard pharmaceutical distribution channels in the Russian Federation. The preparation contained 100 mg of human plasma proteins per 1 mL solution, with IgG comprising at least 97% of the protein content. The formulation included 22.5 mg of glycine (aminoacetic acid) and up to 1 mL water for injection.

Measurement procedure

The complex dielectric permittivity was measured using a Novocontrol Concept 41 spectrometer at the interdisciplinary Resource Center for collective use of Herzen University (Modern Physical and Chemical Methods for the Research and Development of Materials for Industry, Science, and Education). The frequency range spanned from 0.1 Hz to 15 MHz, and measurements were conducted at controlled temperatures between 35 and 39.7 °C.

Data acquisition and analysis were performed using WinDETA software (Novocontrol Technologies GmbH, Germany).

For each temperature, the relaxation parameters (α, β, τ_o) and the relaxation time distribution function $G(\tau)$ were determined via WinFit software (Novocontrol Technologies GmbH & Co). This software employs an approximation algorithm for $\varepsilon''(\omega)$ based on formula (8) and the methodology described earlier.

The measuring cell was a flat capacitor with a 0.24 mm. distance between the plates. The sample volume for each measurement was 5 µL.

Results and discussion

The obtained results

The frequency-dependent dielectric properties $\varepsilon'(f)$, $\varepsilon''(f)$, and $tg\delta$ were measured across the frequency range of 0.1 Hz to 15 MHz at temperatures between 35 and 39.7 °C, with temperature increments of 0.3–0.4 °C.

Figure 1 presents the three-dimensional frequency-temperature dependence of $tg\delta$.
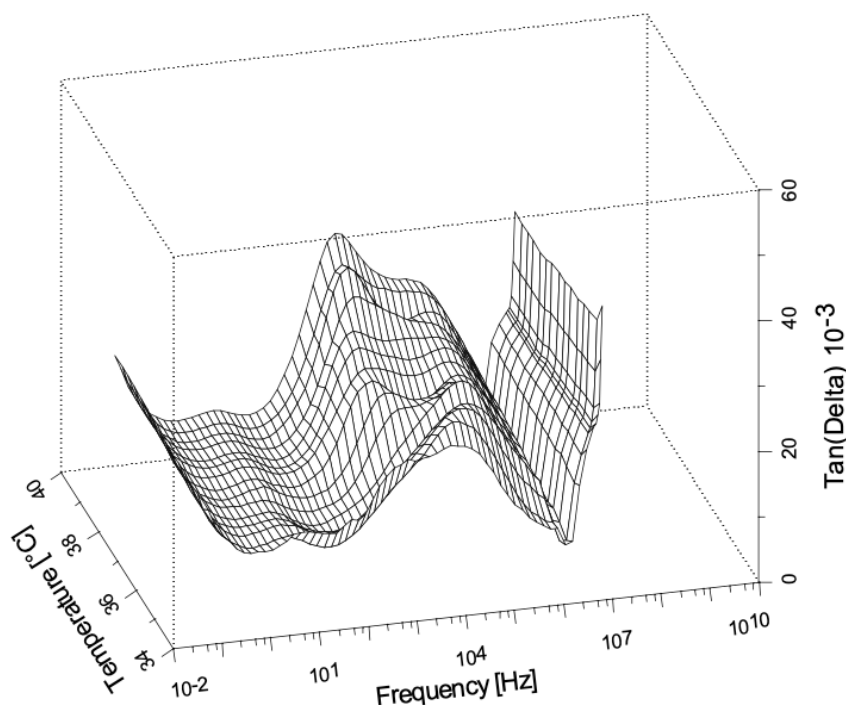
Fig. 1. The value of $tg\delta(f,T)$ at f = 0.1Hz–15 MHz, T = 35–39.7 °C

Figure 2 shows the frequency dependences $\varepsilon'(f)$ for the temperature range of 35–39.7 ^{0}C. Similarly, Figure 3 shows the frequency dependences $\varepsilon''(f)$ across the same temperature range.
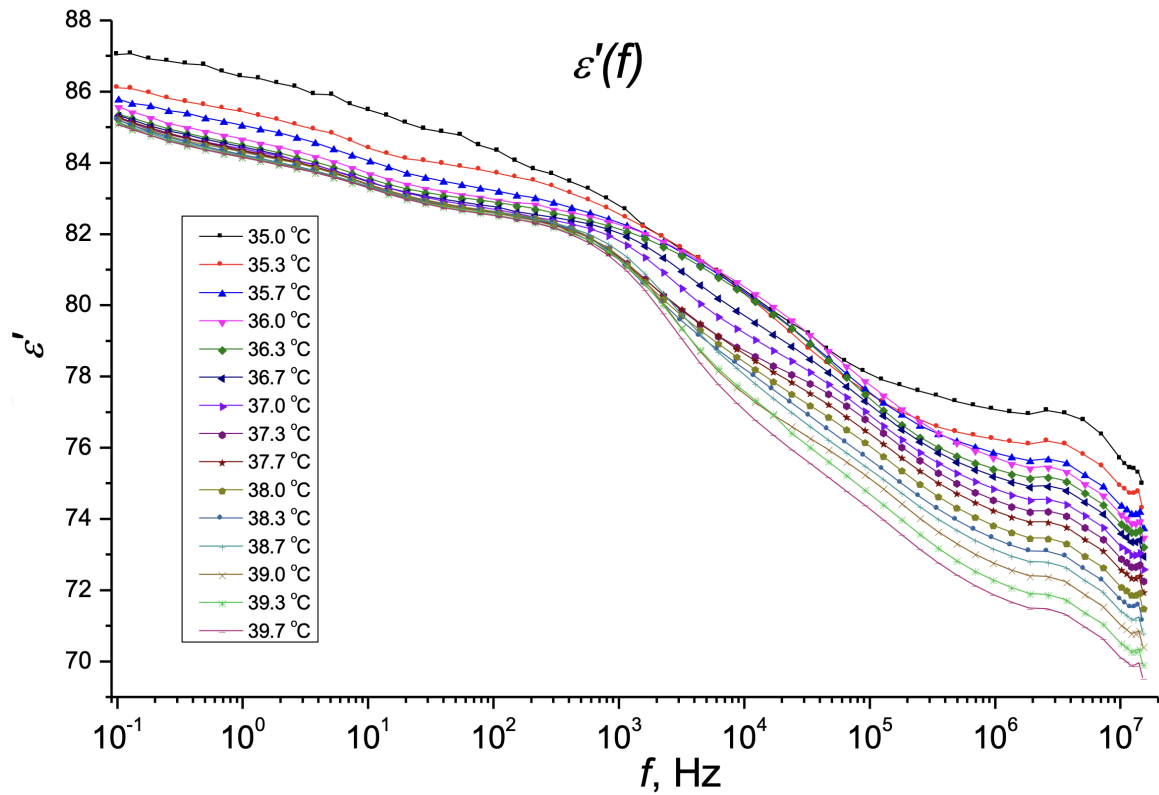
Fig. 2. Frequency dependence of $\varepsilon'(f)$ at T = 35–39.7 °C
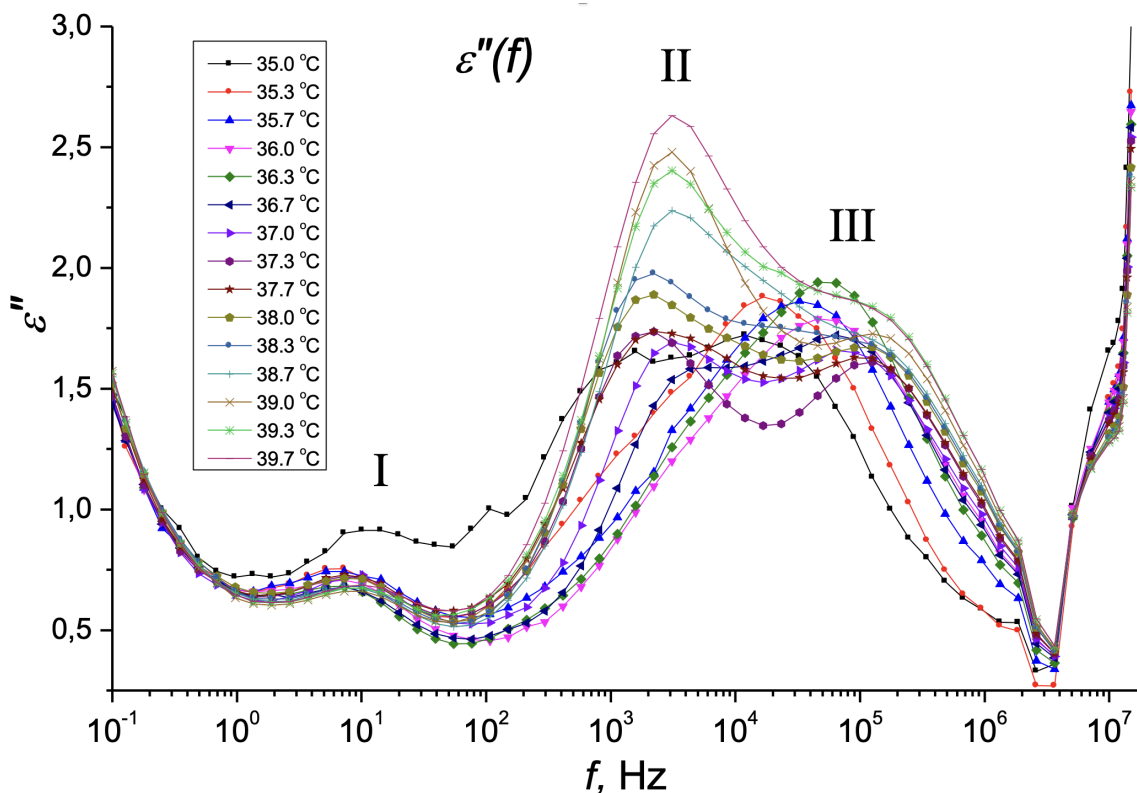
Fig. 3. Frequency dependence $\varepsilon''(f)$ at T = 35–39.7 °C

Figure 3 reveals three distinct relaxation maxima located at approximately $f \approx 10$ Hz, $f \approx 3 \times 10^3$ Hz, and $f \approx 5 \times 10^4$ Hz. Corresponding dispersion regions for $\varepsilon'(f)$ are evident in Figure 2 within these frequency ranges. The shift of the $\varepsilon''(f)$ maxima toward higher frequencies with increasing temperature confirms the relaxation nature of these processes. At the same time, all the three processes partially overlap. The first relaxation process terminates near $f \sim 10^2$ Hz, however, $\varepsilon''(f)$ remains non-zero due to the onset of the second relaxation process. This second process subsequently transitions into the third relaxation process at higher frequencies. Notably, the overlap between the second and third processes is significantly more pronounced than between the first and second processes. At frequencies exceeding 10^7 Hz, an increase in $\varepsilon''(f)$ suggests the presence of an additional relaxation process. However, the absence of a maximum in this frequency range prevents reliable determination of its parameters.

In the low-frequency range of 0.1–1 Hz, an increase in $\varepsilon''(f)$ is also observed. This behavior is either due to significant changes in the sample's electrical conductivity at low frequencies or to the presence of an additional relaxation process.

Figures 4 and 5 show the detailed frequency dependence of $\varepsilon''(f)$ for the first relaxation process (I) across different temperature ranges. A broad, asymmetric maximum is observed at $f \sim 10$ Hz, which narrows with increasing temperature.
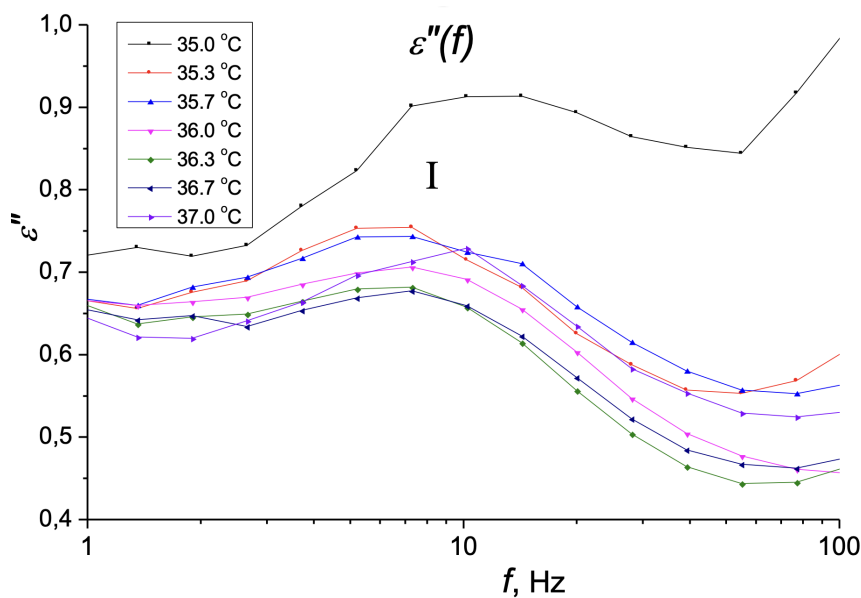
Fig. 4. Frequency dependence $\varepsilon''(f)$ for process I at $T = 35.0$–37.0 °C
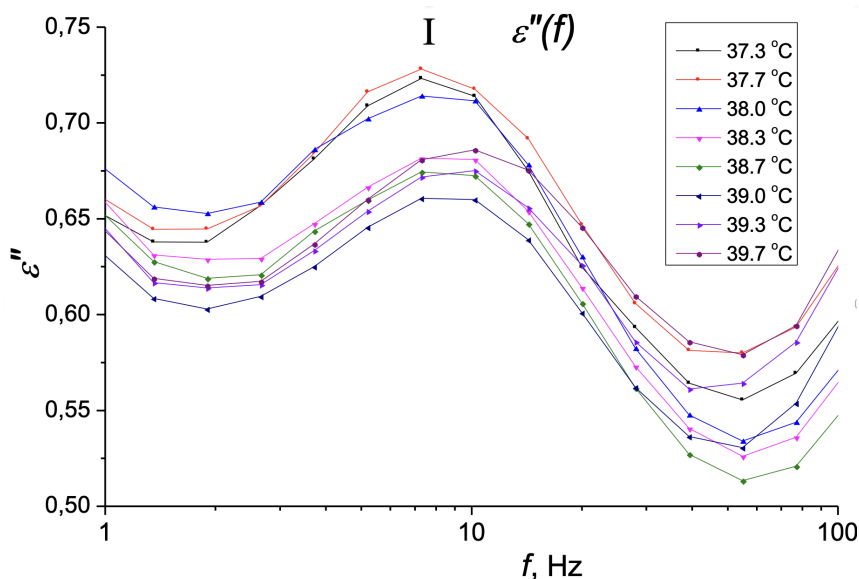
Fig. 5. Frequency dependence $\varepsilon''(f)$ for process I at $T = 37.3$–39.7 °C

Figures 6 and 7 show the detailed frequency dependences of $\varepsilon''(f)$ in the range of 100 Hz to 2 MHz across different temperature ranges. Two partially overlapping relaxation processes (II and III) are observed: process II at $f \sim 3 \times 10^3$ Hz and process III at $f \sim 10^5$ Hz. The maximum values of both processes are three times larger than those of the first process. With increasing temperature, process II becomes more pronounced relative to process III.
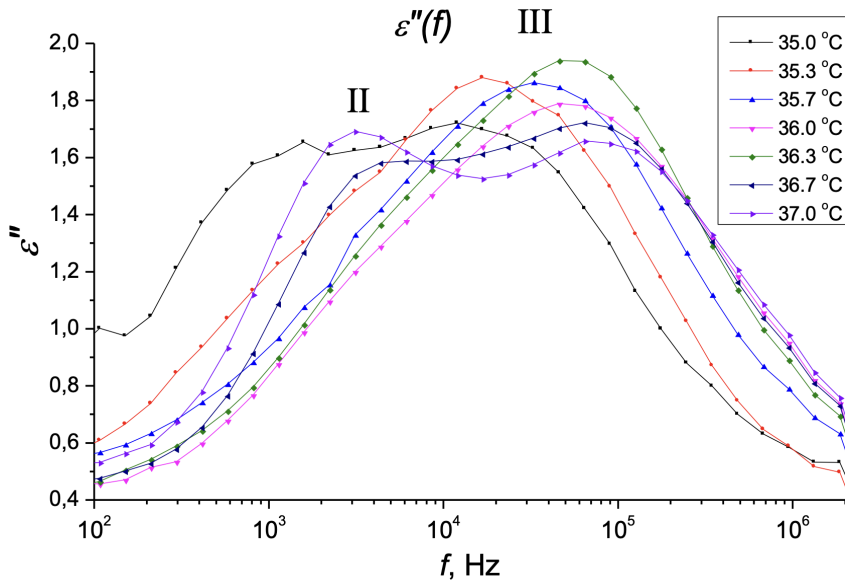
Fig. 6. Frequency dependence $\varepsilon''(f)$ for processes II, III at $T = 35.0$–37.0 ºC
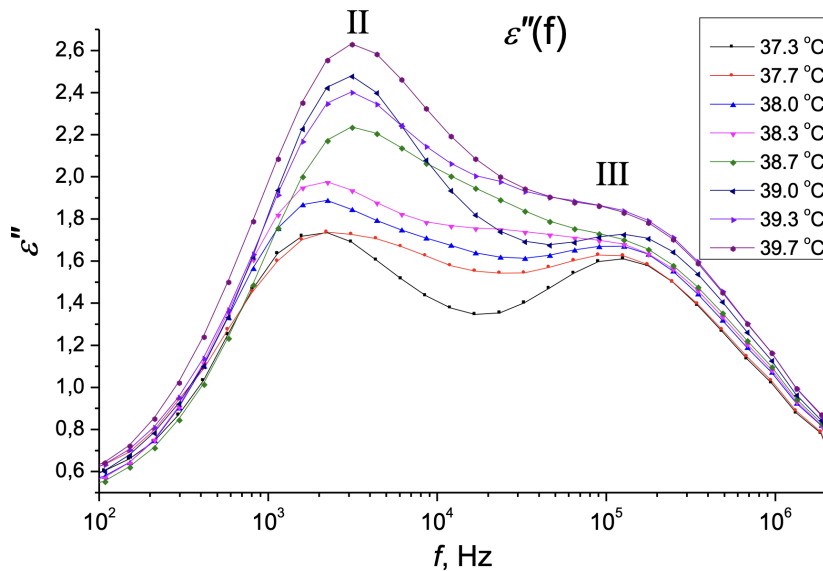
Fig. 7. Frequency dependence $\varepsilon''(f)$ for processes II, III at $T = 37.3$–39.7 ºC

For all observed processes (I, II, III), the relaxation parameters α, β, and τ_0 were determined using the WinFit software following the previously described methodology. The analysis employed the H–N equation (8), which simultaneously accounts for three relaxation processes and electrical conductivity. Experimental data points at frequencies above 2×10^6 Hz were excluded. Figure 8 presents the analysis results for T = 37.3 °C, showing the experimental $\varepsilon''(f)$ data points along with the approximation curve, individual contributions from each relaxation process, and the electrical conductivity at low frequencies. The derived parameters α, β and τ_0 were used to construct the relaxation time distribution function $G(\tau)$, displayed in Figure 9. It shows an overlap between all three relaxation processes (I, II, III).
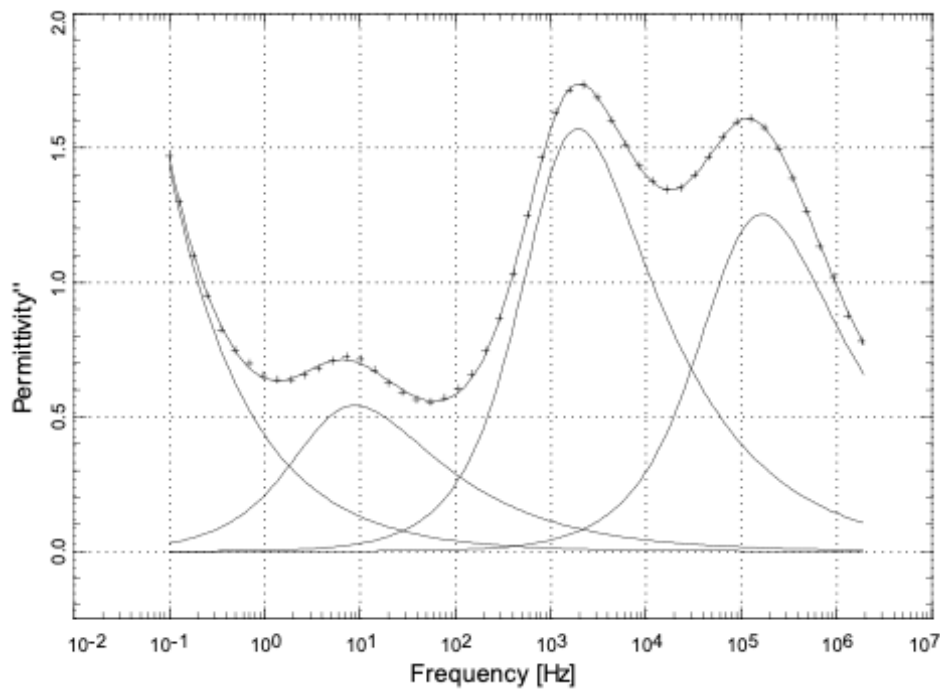
Fig. 8. $\varepsilon''(f)$ at $T = 37.3$ ºC
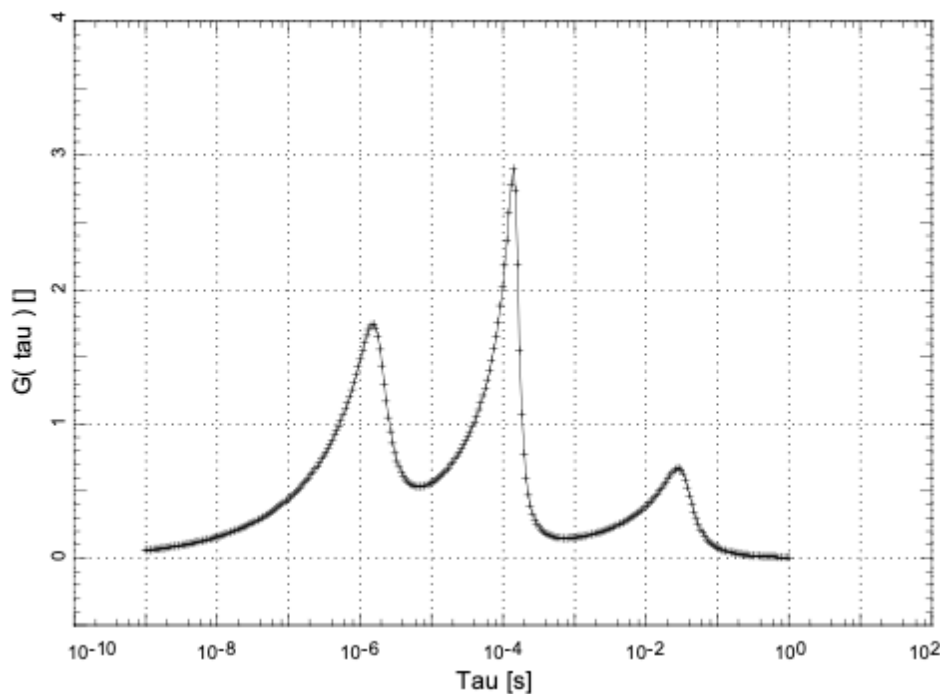
Fig. 9. $G(\tau)$ for Fig. 8

The calculated relaxation parameters (α, β, τ_0) for each process at all temperatures are presented in Table 1. The approximation error for α and β did not exceed 0.04, while for τ_0 it remained below 15%. When α and β values approached 0.00, their error did not exceed 0.02.

Figure 10 shows the Cole-Cole diagrams for different temperatures. The diagrams are asymmetrical in shape, and their centers (if modeled as semicircular arcs) are located below the ε' axis. This graphically confirms the large values of the α and β parameters. At $T = 35$ °C, the diagram differs significantly from those at other temperatures. Studying this phenomenon requires additional data at lower temperatures, which will be presented in future work.

Table 1. Values of relaxation parameters α, β, τ_0 (according to equation 8)

T, ºC	The first (I) relaxation process: $f = 1-100$ Hz			The second (II) relaxation process: $f = 100$ Hz-10 kHz			The third (III) relaxation process: $f = 10$ kHz-1 MHz		
	α_1	β_1	τ_{0_1} (s)	α_2	β_2	τ_{0_2} (s)	α_3	β_3	τ_{0_3} (s)
35.0	0.10	0.74	3.6×10^{-2}	0.00	0.77	3.7×10^{-4}	0.11	0.37	8.7×10^{-6}
35.3	0.13	0.08	2.4×10^{-2}	0.32	0.00	1.3×10^{-4}	0.22	0.43	1.1×10^{-5}
35.7	0.13	0.42	3.4×10^{-2}	0.38	0.08	6.3×10^{-5}	0.25	0.44	6.9×10^{-6}
36.0	0.15	0.42	3.6×10^{-2}	0.32	0.00	3.5×10^{-5}	0.26	0.44	3.6×10^{-6}
36.3	0.00	0.59	4.8×10^{-2}	0.34	0.20	3.7×10^{-5}	0.16	0.47	3.7×10^{-6}
36.7	0.10	0.59	4.2×10^{-2}	0.11	0.29	6.1×10^{-5}	0.20	0.48	3.1×10^{-6}
37.0	0.13	0.51	3.2×10^{-2}	0.08	0.29	7.9×10^{-5}	0.22	0.46	2.7×10^{-6}
37.3	0.12	0.52	3.6×10^{-2}	0.05	0.53	1.6×10^{-4}	0.12	0.51	1.9×10^{-6}
37.7	0.18	0.27	2.5×10^{-2}	0.13	0.67	1.9×10^{-4}	0.16	0.37	1.4×10^{-6}
38.0	0.17	0.35	2.7×10^{-2}	0.00	0.72	2.1×10^{-4}	0.24	0.25	1.2×10^{-6}
38.3	0.18	0.25	2.2×10^{-2}	0.00	0.57	1.7×10^{-4}	0.42	0.00	1.2×10^{-6}
38.7	0.18	0.28	2.4×10^{-2}	0.09	0.53	1.1×10^{-4}	0.38	0.00	8.2×10^{-7}
39.0	0.14	0.49	3.4×10^{-2}	0.10	0.19	7.0×10^{-5}	0.33	0.06	9.3×10^{-7}
39.3	0.26	0.31	2.4×10^{-2}	0.08	0.49	1.1×10^{-4}	0.36	0.00	8.9×10^{-7}
39.7	0.23	0.04	1.7×10^{-2}	0.15	0.29	7.9×10^{-5}	0.33	0.15	1.1×10^{-6}
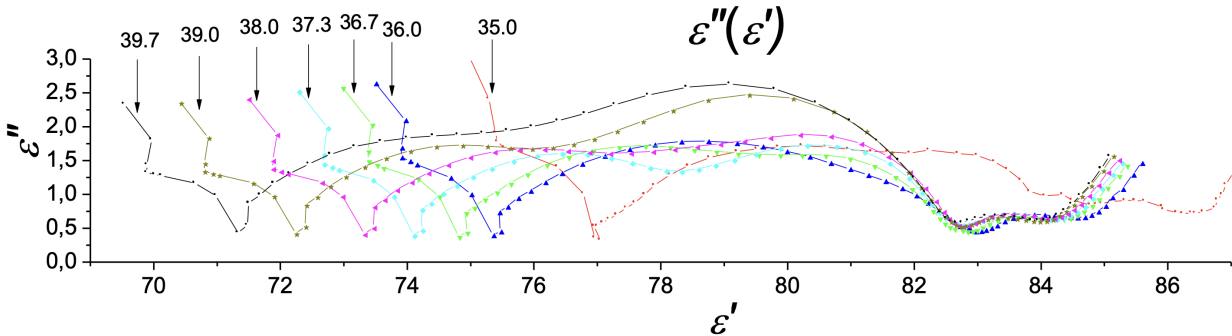
Fig. 10. $\varepsilon''(\varepsilon')$ at $T = 35-39.7$ ºC

Figure 11 presents the function $G(\tau)$ at different temperatures. Three maxima corresponding to three overlapping relaxation processes are visible. The shape of $G(\tau)$ varies with temperature. The decomposition of $G(\tau)$ into components will be presented below (see Figs. 14, 16, 18).

Let us consider the IgG molecule in terms of potential kinetic units responsible for these relaxation processes.

Immunoglobulin G (Litman, Good 1978)

The immunoglobulin G (IgG) molecule is a Y-shaped, globular, water-soluble protein with a molecular weight of 150 kDa. It consists of four polypeptide chains: two light (L) chains (25 kDa each) and two heavy (H) chains (50 kDa each). These chains are covalently linked through interchain disulfide bonds to form a single structure. Figure 12 presents a schematic representation of the IgG molecule.

The quaternary structure of IgG comprises three globular regions: two Fab fragments and one Fc fragment. Each fragment contains four domains: the Fab fragments consist of V_L, V_H and C_L, and C_H1 domains, while the Fc fragment contains two C_H2 and two C_H3 domains. Within these domains, the polypeptide chains primarily adopt β-sheet conformations with parallel folds, while α-helices are essentially absent. The domain geometries shown in Figure 12, along with the dimensions of Fab and Fc fragments, were determined through X-ray diffraction analysis. Crystallographic and hydrodynamic
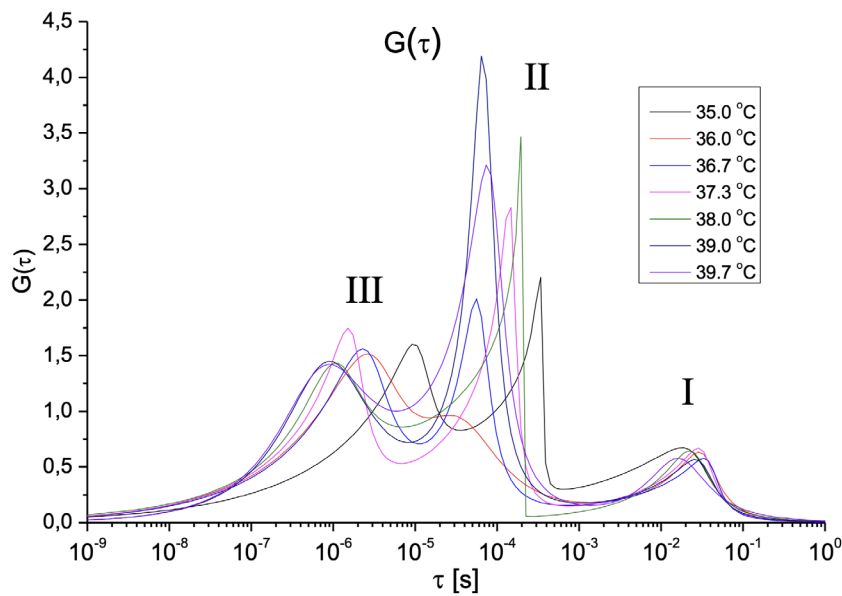
Fig. 11. *G(τ)* at *T* = 35–39.7 ℃
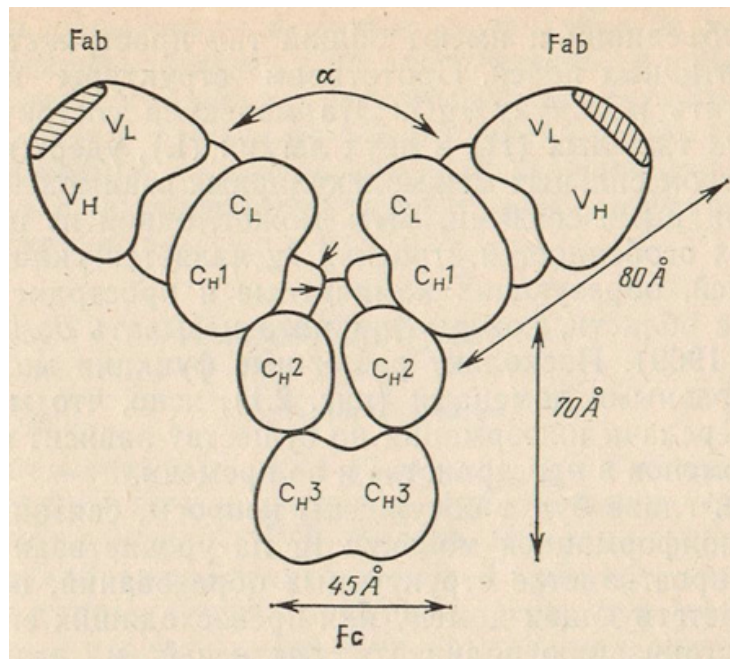
Fig. 12. Schematic representation of the IgG structure. Taken from (Litman, Good 1978, 59)

studies of Fab and Fc fragments reveal that they can be approximated as ellipsoids of revolution with an axial ratio of 2:1, with each Fab fragment exhibiting a relatively large free volume in its central region. Antigen-binding sites are located at the tips of the Fab fragments, indicated in Figure 12 by shaded areas. The Fc fragment contains a hinge region between the two C_H2 domains (indicated by arrows in Figure 12) that enables variation of the angle α between Fab fragments. Typically, this angle exceeds 90–100°. Antigen binding induces conformational changes in the α angle, triggering IgG's biological functions, i. e., the immune response against antigens.

The Fc fragment may adopt an asymmetric position relative to the Fab fragments and need not lie within their plane. This asymmetry can alter the IgG molecule's dipole moment. Within the Fab regions, the non-crystallographic symmetry axes of the V_L, V_H and C_L, and C_H1 domains may form varying angles, further modifying the molecular dipole moment.

These observations demonstrate that the IgG molecule exhibits multiple forms of intramolecular motion across its quaternary, tertiary, secondary, and primary structural elements. These dynamic modes can overlap, giving rise to a broad, composite relaxation process.

Identification of processes

According to established methodology (Gorokhovatskiy et al. 2013, 93), there exist three types of relaxation processes: α, β, and γ. The α-process corresponds to dipole-segmental motion, while β and γ processes represent dipole-group motions. The kinetic units differ for each process type. For the α-process, the kinetic units consist of whole molecules or large segments corresponding to tertiary structural elements. The β-processes involve large polar groups of molecules that vary in size and mass, such as α-helices or β-sheets. The γ-processes are characterized by small polar groups of molecules, including amino acid residues. When different processes possess kinetic units of similar characteristics, they may merge, leading to broadening of the dielectric spectrum. A broad relaxation process typically contains multiple subprocesses: α_1, α_2, α_3 and so on for the α-process and β_1, β_2, β_3 and so on for the β-process. Each subprocess exhibits its own characteristic relaxation time and contributes to the overall observed relaxation behavior (Bartenev, Barteneva, 1992).

In our case, we observe three processes with characteristic relaxation times: I-process $\tau_{0\_1} \approx 10^{-2}$ s., II-process $\tau_{0\_2} \approx 10^{-4}$ s., III-process $\tau_{0\_3} \approx 10^{-6}$ s. We propose that process I is an α-process, while process III corresponds to a β-process. This assignment is justified by their four-order-of-magnitude separation in relaxation times. Furthermore, we suggest that process II may also be classified as a β-process. This interpretation is supported by the temperature-frequency dependence of $tg\delta(f,T)$ shown in Figure 1, where processes II and III appear in close proximity, exhibiting mutual overlap and collectively forming local maxima and minima. Additional evidence comes from Figure 3, which shows increased ε'' values at both low (0.1–1 Hz) and high (5–15 MHz) frequency ranges. We attribute these features to the emergence of additional relaxation processes: potentially another α-process at low frequencies and an additional β-process at high frequencies.

The first relaxation process

The first relaxation process (I) appears in the temperature range $T = 35–39.7$ °C within the frequency domain $f = 1–100$ Hz (Figs. 4, 5). The maximum value of $\varepsilon''(f) \approx 0.7$ is observed at $f \approx 10$ Hz. Figure 13 presents the temperature evolution of relaxation parameters $\alpha_1(T)$ and $\beta_1(T)$ for this process. These dependencies likely reflect conformational changes occurring in the kinetic units responsible for process I.
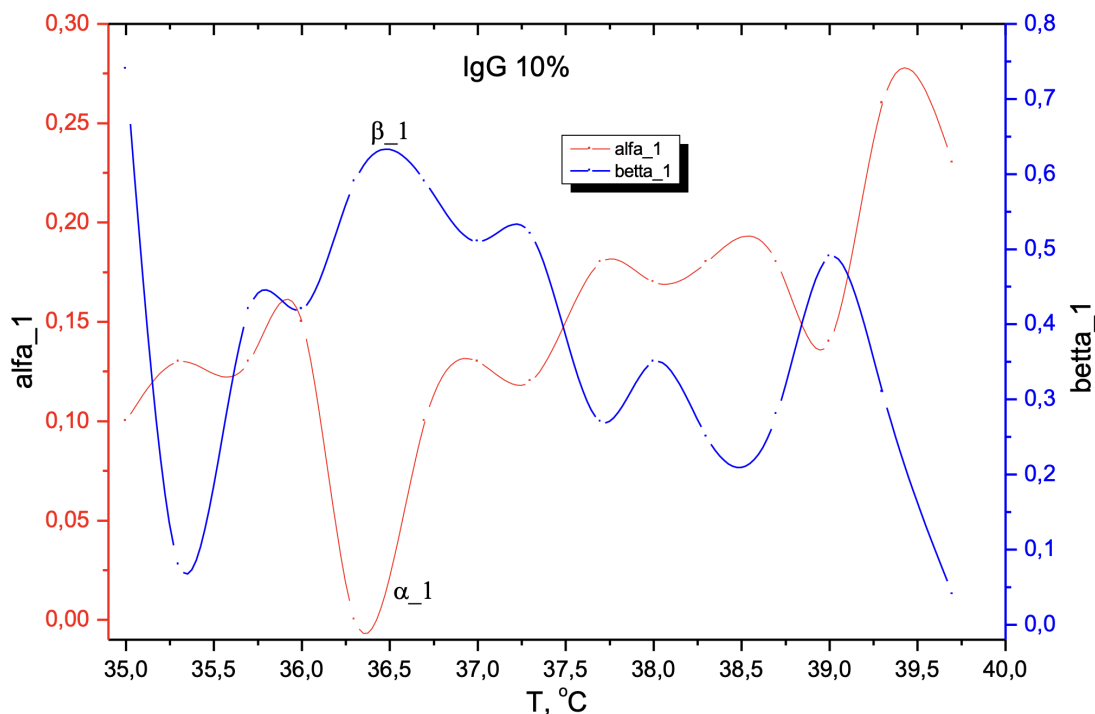
Fig. 13. Temperature dependences of relaxation parameters $\alpha_1(T)$ and $\beta_1(T)$ for the first relaxation process

It can be seen that the minima of $\alpha_1(T)$ correspond to the maxima of $\beta_1(T)$ and vice versa. This reciprocal relationship suggests a connection between these parameters. At $T = 36.3$ °C, this behavior is particularly evident, with α_1 reaching its minimum ($\alpha_1 = 0$) and β_1 attaining its maximum ($\beta_1 = 0.6$). The decrease in α_1 reflects reduced heterogeneity in the sizes and shapes of kinetic units. Concurrently, the elevated β_1 value indicates highly pronounced cooperative motion, where the rotational probability of a kinetic unit becomes strongly dependent on neighboring unit orientations. This simultaneous minimization of α_1 and maximization of β_1 likely signify substantial conformational changes in the kinetic units associated with the first relaxation process. Such changes may potentially involve phase transitions, including globule-to-coil transformations.

The relatively long relaxation time ($\langle\tau_{01}\rangle = 3.1 \times 10^{-2}$ s) indicates that the kinetic units of the first process must be either complete IgG molecules or substantial segments of the tertiary structure, particularly the Fab and Fc fragments. This would classify the first relaxation process as dipole-segmental motion (α-process). To identify the specific structural elements involved, we examine Figure 3, which reveals increased $\varepsilon''(f)$ in the 0.1–1 Hz range. This low-frequency enhancement likely represents an additional relaxation process rather than conductivity effects, suggesting that rotation of entire IgG molecules occurs at even lower frequencies. Consequently, complete IgG molecules cannot be the kinetic units for the first process. We therefore propose that Fab and Fc fragments serve as the kinetic units, with the observed conformational changes arising from modifications in their spatial configuration. The limited response of these fragments to alternating electric fields is evidenced by the modest dielectric loss peak $\varepsilon''(f) \approx 0.7$ (Fig. 3) and the slight polarization change $\Delta\varepsilon'(f) \approx 84 - 83 = 1$ (Fig. 2). This constrained mobility stems from several factors. Fab and Fc fragments approximate rotation ellipsoids (~80×40 Å) with restricted conformational freedom, their relative positions are stabilized by both quaternary structure maintenance forces and strong intermolecular interactions in aqueous environments, and their substantial size combined with extensive hydrogen bonding to surrounding water molecules severely limits rotational freedom.

The relaxation time distribution function $G(\tau)$ (Fig. 11) was decomposed into constituent processes, with the component corresponding to the first process displayed in Figure 14.
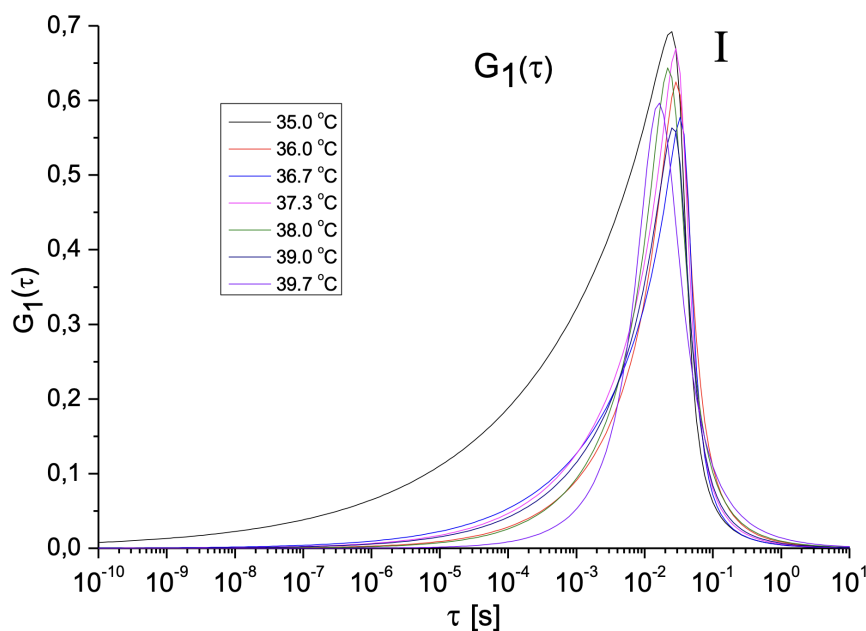
Fig. 14. Relaxation time distribution function $G(\tau)$ for the first relaxation process at various temperatures

The distribution function $G(\tau)$ for the first relaxation process exhibits pronounced asymmetry, as evidenced by $\beta_1 = 0.25$–0.74 The distribution spans six frequency decades (10^{-6} to 1 s), indicating considerable breadth. At 35 °C, $G(\tau)$ shows distinct behavior, which correlates with the exceptionally high $\beta_1 = 0.74$ observed at this temperature. This anomalous behavior may signal the onset of an additional relaxation process, though investigation of lower temperature data would be required for definitive analysis.

The second relaxation process

The second relaxation process (II) occurs in the temperature range $T = 35–39.7$ °C within the frequency domain $f = 100$ Hz–10 kHz (Figs. 6, 7). The maximum value of $\varepsilon''(f) \approx 2–2.5$ is observed at $f \approx 3$ kHz emerging at temperatures $T \geq 36.7$ °C. The peak magnitude shows temperature dependence, increasing from $\varepsilon'' = 1.5$ at $T = 36.7$ °C to $\varepsilon'' = 2.6$ at $T = 39.7$ °C. Figure 15 shows the temperature evolution of relaxation parameters $\alpha_2(T)$ and $\beta_2(T)$ for process II, which likely reflects conformational changes in the associated kinetic units.
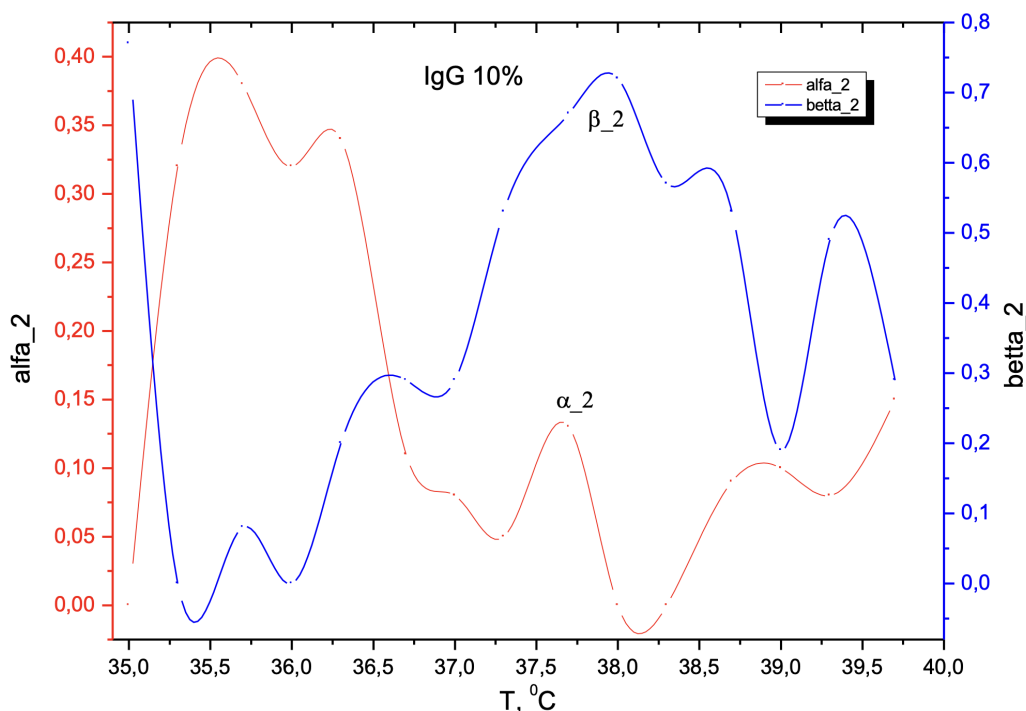
Fig. 15. Temperature dependences of relaxation parameters $\alpha_2(T)$ and $\beta_2(T)$ for the second relaxation process

In the temperature range $T = 36.7–39.7$ °C, this process has a very narrow ($\alpha_2 \approx 0.1$) and asymmetric ($\beta_2 \approx 0.3–0.7$) relaxation spectrum. A particularly notable behavior occurs at 38–38.3 °C, where α_2 reaches zero while β_2 peaks at 0.72, signaling substantial conformational changes in the kinetic units that may involve phase transitions. Figure 15 reveals another significant feature at $T \approx 36$ °C, where α_2 attains its maximum value ($\alpha_2 \approx 0.4$) while β_2 drops to its minimum ($\beta_2 = 0$). This relationship indicates independent rotation of kinetically distinct units. The co-occurrence of maximal α_2 and minimal β_2 values likely reflects another regime of pronounced conformational changes in the kinetic units. These observations suggest that the temperature dependence of $\alpha_2(T)$ and $\beta_2(T)$ reflects conformational dynamics in process II.

The function $G(\tau)$ for process II is shown in Figure 16.

The temperature-dependent evolution of the relaxation function $G(\tau)$ reveals significant conformational changes in the kinetic units of the second process, particularly evident at 35 and 38 °C where the distribution shifts markedly. Across the studied temperature range, $G(\tau)$ for this process spans four frequency decades ($10^{-7}–10^{-3}$ s), notably narrower than the six-decade breadth observed for the first relaxation process (Fig. 14). The shorter characteristic relaxation times ($<\tau_{0\_2}> \approx 10^{-4}$ s versus $<\tau_{0\_1}> \approx 3 \times 10^{-2}$ s) suggest the second process involves smaller structural elements than the Fab and Fc fragments responsible for the first process. The close correlation between the second and third processes (Figs. 6, 7, 11), evidenced by the temperature-dependent transition of their spectral maxima, indicates they share a common physical origin. We propose these processes represent distinct subcomponents (β_1, β_2) of a unified β-process arising from the relative motion of individual IgG domains (Fig. 12). This intramolecular motion can be understood as internal rotation of structural units (Orville-Thomas 1974), where the β-sheet-rich domains (Finkelstein 2014) undergo dipole-group movements.
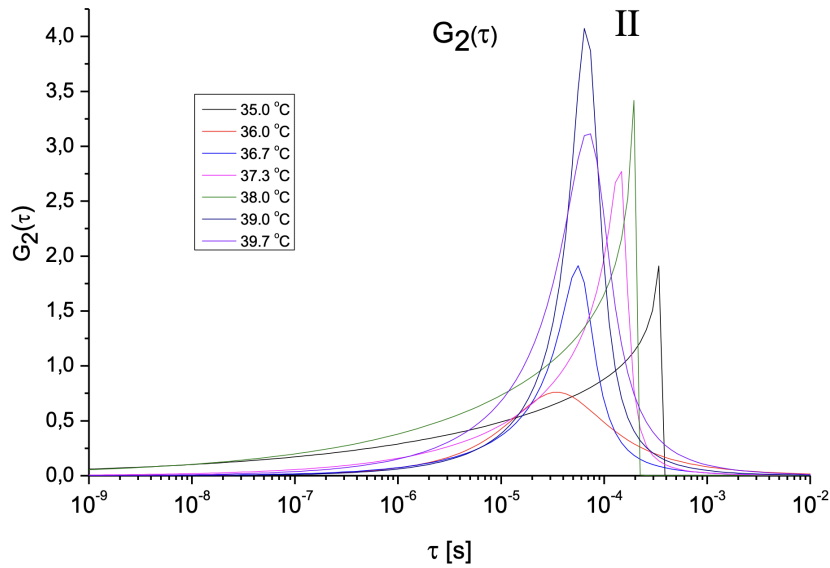
Fig. 16. The time distribution function of the relaxers *G(τ)* for the second relaxation process
at different temperatures

The third relaxation process

The third relaxation process (III) appears in the temperature range T = 35–39.7 °C within the frequency domain f = 10 kHz–1 MHz (Figs. 6, 7). This process exhibits a dielectric loss peak $\varepsilon''(f) \approx 1.5$–1.9 between 35.0 and 38.0 °C, centered at $f \approx 30$–100 kHz. At $T \geq 38.0$ °C (excluding T = 39.0 °C), this peak transforms into an inflection point. The ε'' maximum displays complex temperature dependence: it initially increases (35.0 °C $\leq T \leq$ 36.3 °C), then decreases (36.3 °C $\leq T \leq$ 37.3 °C), before increasing again (37.3 °C $\leq T \leq$ 39.7 °C).

Figure 17 shows the temperature evolution of relaxation parameters $\alpha_3(T)$ and $\beta_3(T)$ for process III.
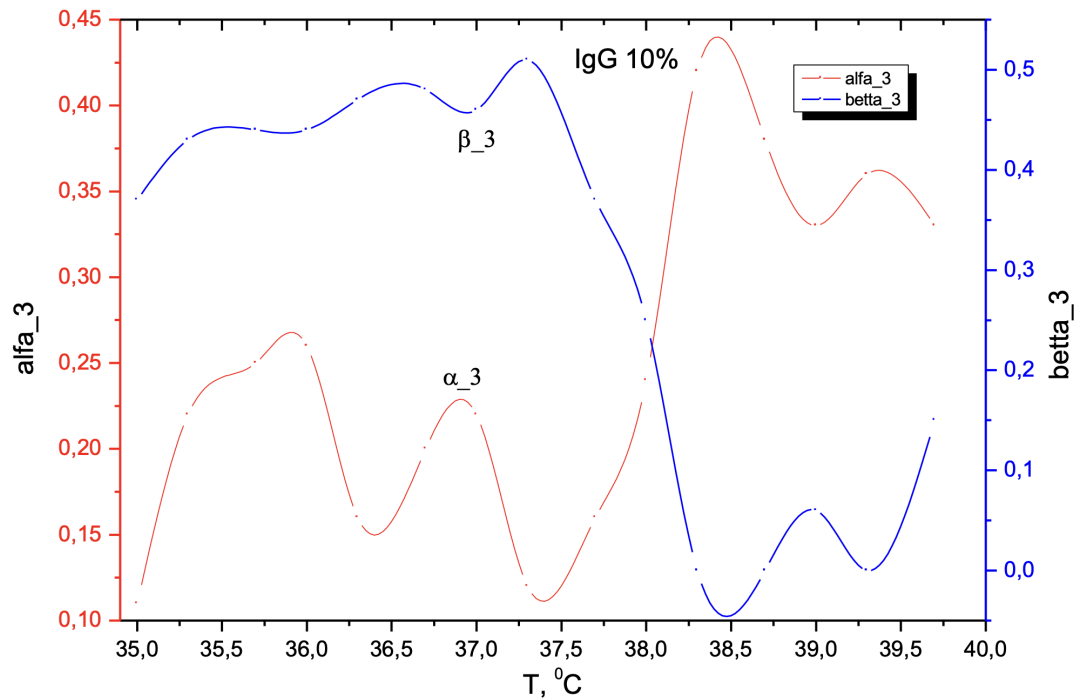
Fig. 17. Temperature dependences of relaxation parameters $\alpha_3(T)$ and $\beta_3(T)$
for the third relaxation process

The parameter α_3 shows two distinct minima, $\alpha_3 = 0.16$ at $T = 36.3$ °C and $\alpha_3 = 0.12$ at $T = 37.3$ °C, corresponding to β_3 maxima of 0.47 and 0.51 respectively. A prominent α_3 maximum of $\alpha_3 \approx 0.44$ occurs at $T \approx 38.4$ °C, accompanied by vanishing ($\beta_3 = 0.0$) at $T = 38.3$–38.7 °C. These parameter variations signify substantial conformational rearrangements in the kinetic units of process III within this temperature range.

The relaxation time distribution function $G(\tau)$ for process III is shown in Figure 18. The distribution spans five decades of frequency (10^{-9}–10^{-4} s), exhibiting greater breadth and symmetry compared to process II (Fig. 18).
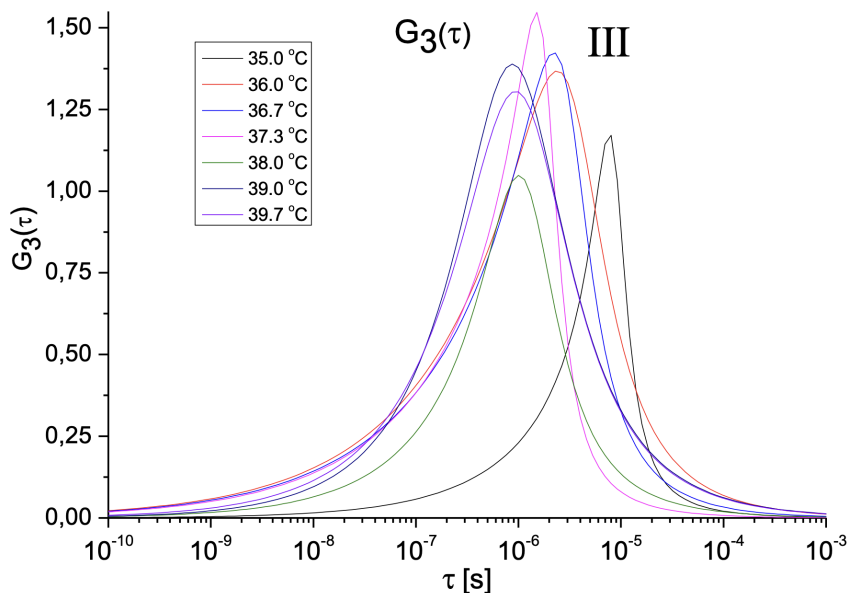
Fig. 18. The time distribution function of the relaxers $G(\tau)$ for the third relaxation process
at different temperatures

As proposed, both the second and third relaxation processes originate from domain motions within the IgG molecule (Fig. 12). However, the third process exhibits significantly shorter relaxation times ($<\tau_{0\_3}> \approx 3 \times 10^{-6}$ s) compared to the second process ($<\tau_{0\_2}> \approx 10^{-4}$ s), reflecting differences in domain size, mass, and intramolecular interactions, as well as available free volume for movement. While Fab fragments contain free volume between the $V_L V_H$ and $C_L C_H 1$ domains enabling larger-scale motions (Fig. 12), the Fc fragment lacks comparable space between $C_H 2$ and $C_H 3$ domains. Thus, the second process involves more extensive domain movements, while the third process consists of restricted, smaller-scale motions. These differences manifest clearly in the relaxation spectra (Figs. 6, 7), with the second process appearing as a stronger, narrower peak compared to the broader, weaker third process. Quantitative analysis in Table 1 confirms this distinction, with the third process showing nearly double the α parameter ($<\alpha_3> = 0.25$ vs $<\alpha_2> = 0.14$) and reduced cooperativity ($<\beta_3> = 0.29$ vs $<\beta_2> = 0.37$).

The broad, asymmetric $G(\tau)$ distributions and large α and β values across all three processes reveal the IgG molecule's complex dynamics, featuring multiple motional scales with distinct activation barriers and characteristic times — a hallmark of protein behavior that can be described as a set of dielectric permittivity with discreet time constants each (Krishtalik 2012).

Possible phase transitions

The anomalous shapes of the relaxation time distribution functions $G(\tau)$ for all three processes (Figs. 19–21) show marked deviations from their typical forms at other temperatures (cf. Figs. 14, 16, 18).

These distinctive profiles, while all resembling the Cyrillic letter 'Λ', demonstrate significant variations in their specific forms — particularly in how abruptly the functions terminate at longer τ values. The corresponding relaxation parameters α and β for these anomalous cases, extracted from Table 1, are presented in Table 2.
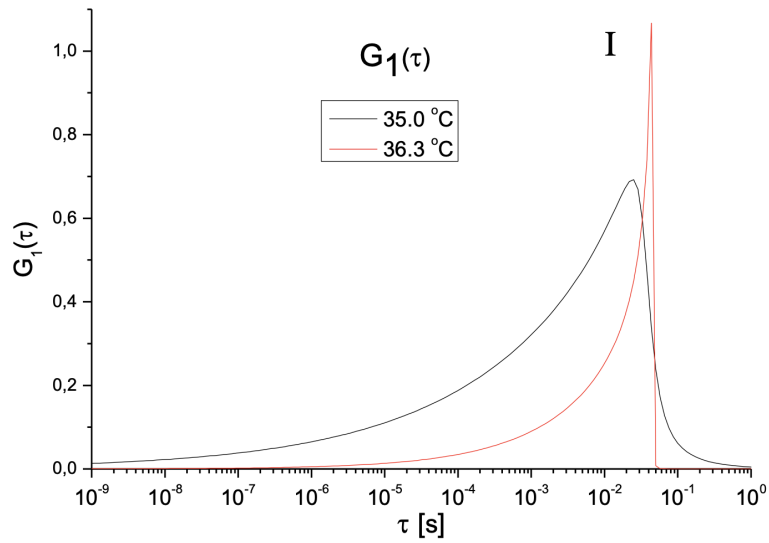
Fig. 19. $G_1(\tau)$ at T = 35.0, 36.3 °C
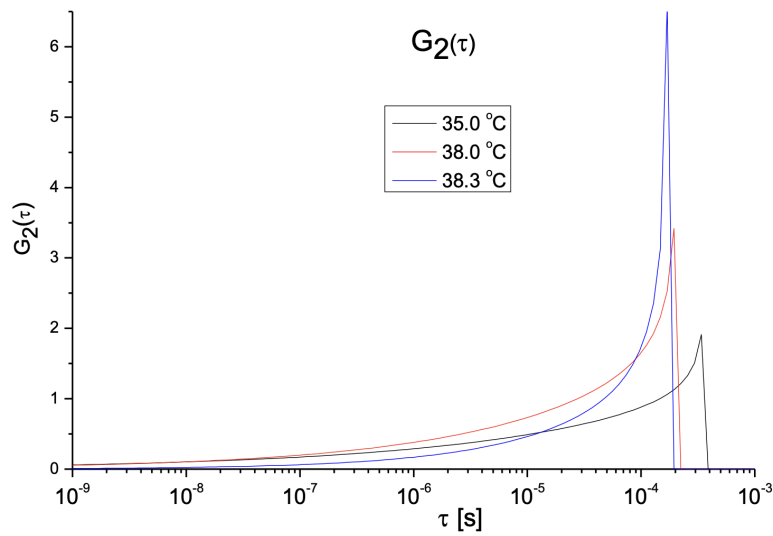
Fig. 20. $G_2(\tau)$ at T = 35.0, 38.0, 38.3 °C
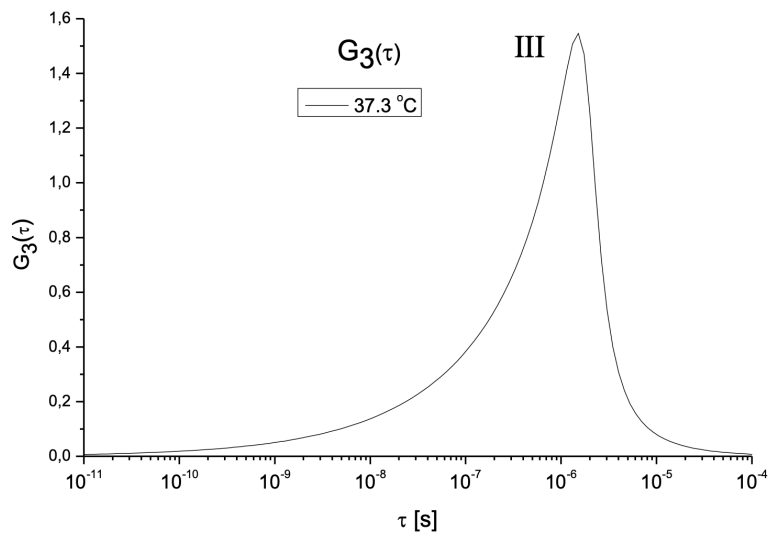
Fig. 21. $G_3(\tau)$ at T = 37.3 °C

Table 2. Values of relaxation parameters α and β for Figs. 19–21

T, ºC	The first relaxation process: f = 1–100Hz		The second relaxation process: f = 100 Hz–10 kHz		The third relaxation process: f = 10kHz–1 MHz	
	α_1	β_1	α_2	β_2	α_3	β_3
35.0	0.10	0.74	0.00	0.77		
36.3	0.00	0.59				
37.3					0.12	0.51
38.0			0.00	0.72		
38.3			0.00	0.57		

The abrupt termination of $G(\tau)$ functions, as observed in Figs. 19–21 ($G_1(\tau)$ at $T = 36.3$ °C, $G_2(\tau)$ at $T = 35.0, 38.0, 38.3$ °C), correlates with two key parameter changes: α approaches zero, while β reaches local maxima (Table 1). This behavior — manifested as a sharp cutoff resembling the Cyrillic 'Λ' shape — suggests the occurrence of a broad phase transition within the $T = 38.0–38.3$ °C temperature range.

We propose that such truncated $G(\tau)$ profiles, accompanied by $\alpha\rightarrow0$ and β maxima, serve as distinctive signatures of phase transitions, where the β magnitude and distribution width (e. g., full width at half maximum) may quantify transition parameters.

Other $G(\tau)$ shapes, like $G_1(\tau)$ at $T = 35.0$ °C (Fig. 19) or $G_3(\tau)$ at $T = 37.3$ °C (Fig. 21), likely reflect substantial conformational changes in kinetic units without constituting true phase transitions.

The theoretical framework for conformational changes and phase transitions in biopolymers has been extensively developed in several monographs (Birshtein, Ptitsyn 1964; Flory 1969; Dashevsky 1987; Grosberg, Khokhlov 1989). The complexity of characterizing these transitions is exemplified by the ongoing debate regarding the classification of the globule-coil transition — while rigid chains exhibit abrupt, first-order transition behavior, flexible chains demonstrate smoother, second-order transitions (Grosberg, Khokhlov 1989, 146).

Recent investigations have employed complementary approaches to study these phenomena: the Shadrin group at Ioffe Institute analyzed the globule-coil transition in albumin through critical exponents (Vonti et al. 2018), while our team (Salnikova et al., 2025) examined the same system via relaxation parameters (α, β) and $G(\tau)$ characteristics. Our studies of 20% aqueous albumin solutions revealed signature behavior during the first relaxation process at $T = 37$ °C — $\alpha_2=0$, maximal β_2 (0.74), and abrupt termination of $G_2(\tau)$ (similar to Fig. 20) — which we interpret as markers of a molecular phase transition.

A qualitative explanation of the detected processes

The physical nature of these relaxation processes stems from temperature-dependent modifications in both intramolecular motions and solvent interactions within the IgG system. As temperature changes, conformational rearrangements occur in various structural elements of the IgG molecule while its interactions with the aqueous environment simultaneously evolve. These alter the dipole-dipole interaction energies, which scale with the squares of the constituent dipole moments (Kaplan 1982, 17). The modified interaction energies change the local electric fields experienced by each kinetic unit, thereby affecting their rotational response to external fields. This directly determines the characteristic temperature and frequency dependences observed in ε' and ε'' components.

Conclusions

Our dielectric spectroscopy study of a 10% aqueous human IgG solution at physiological temperatures identified three characteristic relaxation processes with well-defined parameters. The dominant relaxation (process I) corresponds to the rotational motion of Fab and Fc fragments under the applied alternating electric field, while processes II and III, sharing a common physical origin, reflect intramolecular domain movements within these structural elements.

The temperature-dependent behavior of the relaxation parameters α and β provides new insights into conformational changes of the kinetic units, with the characteristic combination of α approaching zero while β reaches maximum values serving as a potential indicator of phase transitions.

The dielectric spectroscopy approach proves particularly valuable for such investigations due to its inherent sensitivity to dipole moment variations, conformational changes in structural subunits, and modifications in intermolecular interactions within the aqueous environment. This methodology offers a powerful tool for probing relaxation mechanisms in complex fluids, including biological ones.

Conflict of Interest

The authors declare that they have no conflict of interest.

Author Contributions

All the authors discussed the final work and took their respective part in writing the article.

References

Annus, P., Min, M. (eds.). (2021) *Bioimpedance and Spectroscopy.* New York: Academic Press, 454 p. (In English)

Bartenev, G. M., Barteneva, A. G. (1992) *Relaksatsionnye svojstva polimerov [Relaxation properties of polymers].* Moscow: Khimiya Publ., 384 p. (In Russian)

Birshtein, T. M., Ptitsyn, O. B. (1964) *Konformatsii makromolekul [Conformations of macromolecules].* Moscow: Nauka Publ., 392 p. (In Russian)

Blythe, T., Bloor, D. (2005) *Electrical properties of polymers.* 2nd ed. Cambridge: Cambridge University Publ., 506 p. (In English)

Borisova, M. E., Kojkov, S. N. (1979) *Fizika dielektrikov [Physics of dielectrics].* Leningrad: Leningrad State University Publ., 240 p. (In Russian)

Dashevsky, V. G. (1987) *Konformatsionnij analiz makromolekul [Conformational analysis of macromolecules].* Moscow: Nauka Publ., 288 p. (In Russian)

Finkelstein, A. V. (2014) *Fizika belkovykh molekul [Physics of protein molecules].* Moscow; Izhevsk: Institute of Computer Research Publ., 424 p. (In Russian)

Flory, P. J. (1969) *Statistical mechanics of chain molecules.* New York; London; Sydney; Toronto: John Wiley & Sons Publ., 440 p. (In English)

Fröhlich, H. (1958) *Theory of dielectrics. Dielectric constant and dielectric loss. 2nd ed.* Oxford: Clarendon Press, 194 p. (In English)

Gorokhovatskiy, Yu. A., Karulina, E. A., Temnov, D. E. (2013) *Fizika polimernikh dielektrikov [Physics of polymer dielectrics].* Saint Petersburg: Herzen State Pedagogical University of Russia Publ., 124 p. (In Russian)

Gotlib, Y. I., Darinskj, A. A., Svetlov, Yu. E. (1986) *Fizicheskaya kinetika makromolekul [Physical kinetics of macromolecules].* Leningrad: Khimiya Publ., 272 p. (In Russian)

Grosberg, A. Yu., Khokhlov, A. R. (1989) *Statisticheskaya fizika makromolekul [Statistical physics of macromolecules].* Moscow: Nauka Publ., 344 p. (In Russian)

Kaplan, I. G. (1982) *Vvedenie v teoriyu mezhmolekularnykh vzaimodejstvij [Introduction to the theory of intermolecular interactions].* Moscow: Nauka Publ., 312 p. (In Russian)

Kremer, F., Schönhals, A. (eds.). (2003) *Broadband dielectric spectroscopy.* Berlin; Heidelberg: Springer Publ., 729 p. https://doi.org/10.1007/978-3-642-56120-7 (In English)

Krishtalik, L. I. (2012) Belki kak spetsificheskaya polyarnaya sreda protsessov perenosa zaryada [Proteins as a specific polar medium of charge transfer processes]. *Uspexi Fizicheskix Nauk — Physics–Uspekhi*, 182 (12), 1275–1300. https://doi.org/10.3367/UFNr.0182.201212b.1275 (In Russian)

Litman, G. W., Good, R. A. (eds.) (1978) *Immunoglobulins.* New York; London: Plenum Medical Book Company Publ., 410 p. (In English)

Orville-Thomas, W. J. (ed.). (1974) *Internal rotation in molecules.* New York; London; Sydney; Toronto: John Wiley & Sons Publ., 606 p. (In English)

Raicu, V., Feldman, Y. (eds.). (2015) *Dielectric Relaxation in biological systems: Physical principles, methods, and applications.* Oxford: Oxford University Press, 388 p. (In English).

Salnikova, Zh. A., Kononov, A. A. (2020) Derivation of the Havriliak—Negami equation for the complex electrical modulus. *AIP Conference Proceedings*, 2308 (1), 030017. https://doi.org/10.1063/5.0034028 (In English)

Salnikova, Zh. A., Kononov, A. A., Smirnov, A. P., Castro, R. A. (2025) Shirokopolosnaya dielektricheskaya spektroskopiya rastvora albumina cheloveka pri fiziologicheskikh temperaturakh [Broadband dielectric spectroscopy of human albumin solution at physiological temperatures]. *Zhurnal Tekhnicheskoj fiziki — Technical Physics*, 95 (6), 1224–1233. https://doi.org/10.61011/JTF.2025.06.60474.427-24 (In Russian)

Sazhin, B. I. (1986) (ed.). *Elektricheskie svojstva polimerov [Electrical properties of polymers].* 3rd ed. Leningrad: Khimiya Publ., 224 p. (In Russian)

Vonti, A. O., Ilyinsky, A. V., Kapralova, V. M., Shadrin, E. B. (2018) Kompleksnaya priroda termicheskikh fazovykh prevraschenij v rastvorakh al'bumina [The complex nature of thermal phase transformations in albumin solutions]. *Zhurnal Tekhnicheskoj fiziki — Technical Physics*, 88 (6), 934–942. (In Russian)